NeuroImage 276 (2023) 120193

Contents lists available at ScienceDirect

NeuroImage

journal homepage: www.elsevier.com/locate/neuroimage

Neurochemistry-enriched dynamic causal models of magnetoencephalography, using magnetic resonance spectroscopy

Amirhossein Jafarian[a,b], Laura E Hughes[a,b], Natalie E Adams[a], Juliette H Lanskey[b], Michelle Naessens[a,b], Matthew A Rouse[a,b], Alexander G Murley[a], Karl J Friston[c], James B Rowe[a,b,*]

[a] Department of Clinical Neurosciences and Cambridge University Hospitals NHS Trust, University of Cambridge, United Kingdom
[b] MRC Cognition and Brain Sciences Unit, University of Cambridge, Cambridge, UK
[c] The Wellcome Centre for Human Neuroimaging, UCL Queen Square Institute of Neurology, United Kingdom

ARTICLE INFO

Keywords:
Dynamic causal modelling
Canonical microcircuits
Bayesian model reduction
parametric empirical Bayes
Magnetoencephalography
Magnetic resonance spectroscopy

ABSTRACT

We present a hierarchical empirical Bayesian framework for testing hypotheses about neurotransmitters' concertation as empirical prior for synaptic physiology using ultra-high field magnetic resonance spectroscopy (7T-MRS) and magnetoencephalography data (MEG). A first level dynamic causal modelling of cortical microcircuits is used to infer the connectivity parameters of a generative model of individuals' neurophysiological observations. At the second level, individuals' 7T-MRS estimates of regional neurotransmitter concentration supply empirical priors on synaptic connectivity. We compare the group-wise evidence for alternative empirical priors, defined by monotonic functions of spectroscopic estimates, on subsets of synaptic connections. For efficiency and reproducibility, we used Bayesian model reduction (BMR), parametric empirical Bayes and variational Bayesian inversion. In particular, we used Bayesian model reduction to compare alternative model evidence of how spectroscopic neurotransmitter measures inform estimates of synaptic connectivity. This identifies the subset of synaptic connections that are influenced by individual differences in neurotransmitter levels, as measured by 7T-MRS. We demonstrate the method using resting-state MEG (i.e., task-free recording) and 7T-MRS data from healthy adults. Our results confirm the hypotheses that GABA concentration influences local recurrent inhibitory intrinsic connectivity in deep and superficial cortical layers, while glutamate influences the excitatory connections between superficial and deep layers and connections from superficial to inhibitory interneurons. Using within-subject split-sampling of the MEG dataset (i.e., validation by means of a held-out dataset), we show that model comparison for hypothesis testing can be highly reliable. The method is suitable for applications with magnetoencephalography or electroencephalography, and is well-suited to reveal the mechanisms of neurological and psychiatric disorders, including responses to psychopharmacological interventions.

1. Introduction

This paper introduces an empirical Bayesian methodology for inferring synaptic physiology from human, in vivo neurophysiological recordings and in vivo measurements of neurochemicals, including neurotransmitters. It is an example of a broader class of enriched dynamic causal models (DCMs), informed by multimodal data that can incorporate neurochemistry, molecular pathology or selective loss of neuronal sub-populations and their synapses. Magnetic resonance spectroscopy (MRS) can be used to estimate individual differences in key neurochemical concentrations in local brain regions (Blüml and Panigrahy, 2012). It has been used to quantify neurochemical changes in neurological and neuropsychiatric disorders, such as Alzheimer's disease (Wang et al., 2015), frontotemporal lobar degeneration-related syndromes (Murley et al., 2020; Murley et al., 2022), and schizophrenia (Jelen et al., 2018; Cohen et al., 2015; Duarte and Xin, 2019), as well as normal ageing (Boumezbeur et al., 2010). Such spectroscopy can be predictive of task performance and the response to pharmacological interventions (Chowdhury et al., 2012; Stagg et al., 2011; McColgan et al., 2020; Gawne et al., 2020; Schmitz et al., 2017;

* Corresponding author at: Cambridge Centre for Frontotemporal Dementia, Department of Clinical Neurosciences, University of Cambridge, Herchel Smith Building, Forvie Site, Robinson Way, Cambridge Biomedical Campus, Cambridge, CB2 0SZ, UK

E-mail addresses: aj631@cam.ac.uk (A. Jafarian), laura.hughes@mrc-cbu.cam.ac.uk (L.E. Hughes), tallie.adams@gmail.com (N.E. Adams), juliette.lanskey@mrc-cbu.cam.ac.uk (J.H. Lanskey), mln37@medschl.cam.ac.uk (M. Naessens), matthew.rouse@mrc-cbu.cam.ac.uk (M.A. Rouse), am2505@medschl.cam.ac.uk (A.G. Murley), k.friston@ucl.ac.uk (K.J. Friston), james.rowe@mrc-cbu.cam.ac.uk (J.B. Rowe).

https://doi.org/10.1016/j.neuroimage.2023.120193.
Received 24 October 2022; Received in revised form 11 May 2023; Accepted 24 May 2023
Available online 26 May 2023.

Adams et al., 2021). Differences in neurotransmitter levels influence synaptic transmission, which in turn affects the generators of magneto- and electro-encephalographic signals (M/EEG).

Here, we characterise the relationship between physiology and neurotransmitter levels, using a hierarchical Bayesian approach (Friston et al., 2016). We present a method for specifying and comparing the evidence for hierarchical models (using parametric empirical Bayes) that encode the effect of neurotransmitter levels (as measured with MRS) as empirical priors on different combinations of synaptic parameters in a neural mass model of MEG recordings. Our approach complements previous studies, where correlational analysis has been used to investigate relationships between spectroscopy measures and electrophysiology (Rideaux, 2021; Steel et al., 2020; Kober et al., 2001). We envisage that our method may be useful for characterising the synaptic deficits in several neuropsychiatric conditions (e.g., (Adams et al., 2021; Limongi et al., 2021)).

MRS is a non-invasive neuroimaging modality used to estimate biochemical concentrations, including the neurotransmitters glutamate and gamma-aminobutyric acid (GABA) (McColgan et al., 2020; Stagg and Rothman, 2013). Glutamatergic neurotransmission mechanisms include release, reuptake into astrocytes, conversion to glutamine then glutamate, and vesicular repacking (Gruetter et al., 2001; Pellerin et al., 2007; van der Graaf, 2010). In contrast, GABA cycling is predominantly neuronal where, following a release phase, there is presynaptic GABA reuptake and vesicular repackaging (Gruetter et al., 2001). The majority of GABA and glutamate is intracellular (Myers et al., 2014), but total GABA and glutamate concentrations correlate with neurophysiological features such as gamma oscillatory power and corticospinal excitability (Lally et al., 2014; Greenhouse et al., 2017).

In what follows, we show that neurotransmitter levels can be used as prior constraints on the estimation of effective synaptic connectivity, in biophysically informed models of cortical function. For example, glutamate and GABA concentrations are expected a priori to influence the dynamics of excitatory amino-3-hydroxy-5-methyl-4-isoxazolepropionic acid (AMPA) receptors and inhibitory GABAergic receptors respectively (Rideaux, 2020; Gruetter et al., 2001). The aim of the current work was to compare the evidence for alternate hypotheses regarding the relationships between glutamate/GABA concentrations and synaptic connectivity, quantified using non-invasive MRS recordings and M/EEG data, respectively.

The first step in establishing this relationship is to infer synaptic parameters from neurophysiological observations. Since Hodgkin and Huxley (Hodgkin and Huxley, 1952), there have been many approaches to examine micro-, meso- and macroscale brain dynamics with many options for model identification (Nelson and Rinzel, 1998; Steyn-Ross and Steyn-Ross, 2010; Robinson et al., 2003; Terry et al., 2022; Jirsa et al., 2014; Deco et al., 2008; Ramezanian-Panahi et al., 2022). DCMs build directly on the modelling framework established by Hodgkin and Huxley. Hodgkin and Huxley initially proposed a linear dynamical system model to explain the relation between conductance dynamics and ion current dynamics. However, they refined their model by inclusion of nonlinear dynamics, having considered balancing complexity with accuracy in a way that remains highly relevant to DCM (Nelson and Rinzel, 1998). The hypothesis testing machinery in DCM—enabling inferences on the posterior distributions of neuronal model parameters—balances model complexity and accuracy in generative (i.e., forward) models of neuroimaging data. The open source platform of DCM allows researchers from diverse disciplines to formulate hypotheses and test them within a fairly standard framework. As discussed by (Moran et al., 2013) DCM can be applied for a wide range of models, from the mesoscale and mean field modelling (Marreiros et al., 2015; Marreiros et al., 2009; Marreiros et al., 2010; Shine et al., 2021; Gilbert et al., 2016) to macroscale population dynamics such as COVID-19 transmission (Friston et al., 2022; Friston et al., 2020). Here, we focus on the use of DCM to characterise mesoscale neural dynamics. The mesoscale granularity, afforded by mean field approximations, increases the marginal likelihood of DCMs (i.e., with high accuracy and relatively low model complexity).

We use dynamic causal modelling to invert a canonical microcircuit model of resting state MEG data in healthy adults (Friston et al., 2012; Friston et al., 2003). This entails the variational Bayesian inversion of biologically-informed forward models of neurophysiological observations, under the Laplace assumption; i.e., assuming Gaussian posterior probabilities over unknown parameters (Zeidman et al., 2022; Friston et al., 2007). In DCM, gradient optimisation of variational free energy is used for approximating the posterior probability density over unknown model parameters, and the model evidence (i.e. marginal likelihood) (Friston et al., 2007; Friston et al., 2008). The free energy provides a lower bound on log-model evidence, which represents the model accuracy adjusted for complexity. Model evidence associated with alternate hypotheses—about the underlying generators of data—are compared using Bayesian model reduction (BMR). This identifies the most likely explanation for the empirical data (Kass and Raftery, 1995; Friston and Penny, 2011). Crucially, BMR enables the computationally efficient evaluation of posteriors and model evidence under a reduced prior; i.e., a model specified in terms of new prior constraints (Friston et al., 2018; Friston and Penny, 2011). We estimate the parameters and evidence for a full model of a given dataset and then use BMR to evaluate posteriors and model evidences under alternative priors (Friston et al., 2018; Friston and Penny, 2011; Friston et al., 2019). At the second (e.g., group) level, hierarchical or parametric empirical Bayes (PEB) allows one to include empirical priors of interest (Friston et al., 2015; Friston et al., 2016). Usually, second level models apply priors that are conserved over multiple participants. This means the first level corresponds to a within-subject analysis, while the second level is a between-subject or group analysis (using subject specific posterior estimates as inferred by the first level). The combined hierarchical model can then be assessed in terms of its evidence, and subjected to BMR to test different hypothesis at the within-subject or between-subject level. Note that this hierarchical Bayesian approach—to optimise generative models of neurophysiology, via minimisation of free energy—is not simply correlation or "fitting" data to a model. The free energy provides a bound on model evidence (a.k.a., marginal likelihood) that incorporates model complexity. Maximising evidence therefore protects against poor generalisation (cf. "over-fitting") at first and second levels. Although Bayesian statistics do not feature frequentist type II errors, there is a conceptual analogue in the precision of the data, such that underpowered studies lack sufficient precision to evince differences in model evidence. Practically, insufficient or noisy data reduces the differences in the evidence for one model relative to another; meaning that one could not make a definitive inference about which is the better model given the data to hand.

In DCM, the prior mean and covariance of unknown parameters are specified to accommodate physiological interpretability and model stability, respectively. Effectively, (informative) priors provide constraints that enable the inversion of otherwise over-parameterised models (Friston et al., 2003). Using DCM, differences amongst individuals (or groups) can be characterised in terms of *post hoc* associations between connectivity parameters and clinical, pathological or cognitive measure of interest, or by differential model evidence, or conditional densities over models' probabilities (Adams et al., 2021; Stephan et al., 2009; Rae et al., 2016; Passamonti et al., 2012). However, a more principled Bayesian methodology is to incorporate between-subject variables as priors on the generative model of brain physiology. Bayesian model reduction and group-DCM can then be used to test whether such (empirical) priors increase model evidence compared to conventional (or weakly informative) priors. The source of empirical priors could be demographics (e.g. age), the burden of neuropathology (e.g. from PET scanning), or multi-modal measure (e.g. MRS). In this study, the DCM (at the first and group levels) leverages the spectroscopy information to impose constraints on synaptic physiology and assess their 'goodness' in terms of model evidence. If the embedding of empirical priors into a

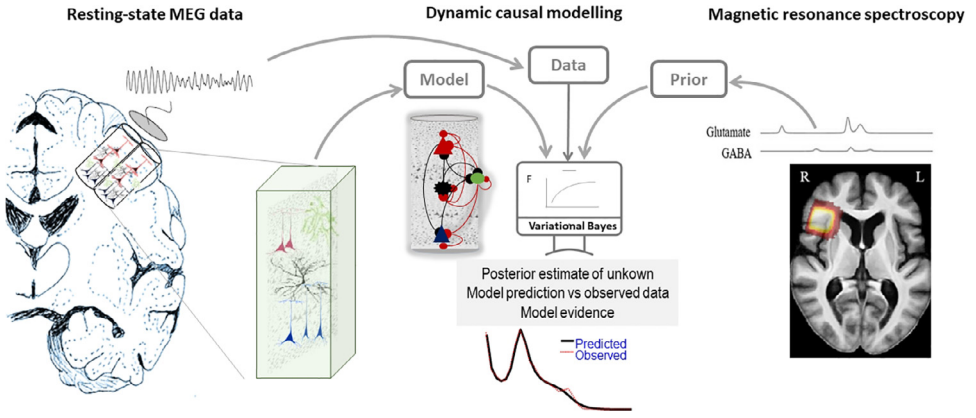

Fig. 1. Dynamic causal modelling (DCM) can be informed by physiological or pathophysiological measures. DCM is the variational Bayesian inversion of mesoscale biologically-informed models given neuroimaging data: e.g., MEG. Given some data, DCM infers unknown synaptic parameters under a given (physically plausible) model and estimates the evidence for that model. The DCM parameter estimates can be informed by empirical priors; here, based on neurotransmitter concentration, as measured by magnetic resonance spectroscopy. Neurotransmitter concentration is proposed to inform the synaptic efficacy in the neural mass model that, in turn, generates electromagnetic signals. The comparison of such empirical priors — in terms of model evidence — extends Bayesian inferences about aspects of brain physiology which cannot be otherwise captured by non-invasive functional neuroimaging. The effect of the neurotransmitter concentration might manifest on one or more classes of synaptic connections in the cortical microcircuit. By specifying which parameters are subject to empirical priors, one can then compare ensuing models to identify which kinds of synaptic connections are modulated by neurotransmitter concentrations. The MRS traces and heatmap are from (Murley et al., 2020) with permission. . Brain icon by Gloria Maggioli from thenounproject.com, CC BY 3.

DCM leads to higher model evidence, one can infer the importance of the measured process in the generation of observed neurophysiology. We use MRS data, noting that GABA and glutamate changes are associated with many neurological conditions.

In this paper, we compare the evidence for different hypotheses about the association between MRS estimates of neurotransmitter concentration and synaptic function. See Fig. 1 for an overview of the method. For a given set of connections, we use a hierarchical optimisation (a greedy search followed by a constrained optimisation) to identify the (linear or nonlinear) function of the MRS estimates—imposing prior constraints—that maximises model evidence at the group level. We then use model reduction to determine which subsets of synaptic parameters are sensitive to individual differences in neurotransmitter concentration. This approach complements previous work by (Stephan et al., 2009; Sokolov et al., 2019) who used diffusion-weighted imaging tractography as empirical priors on connectivity parameters that are inferred from functional magnetic resonance imaging time series. However, unlike previous work, we do not assume a one-to-one relation between MRS measures and connections in the generative model. Rather, we seek evidence to find which synaptic connections are informed by the empirical measures.

This work complements Stephan et al. (2009) contribution in which anatomical DTI data were used to furnish empirical priors in single-subject DCMs. In the current paper, empirical MRS measures do not directly inform the first-level DCM priors; in contrast they are used as 'covariates' in the second-level design matrix of PEB (group DCM) that parameterise alternative relationships between MRS values and subsets of first-level DCM parameters. This, in turn, allows one to evaluate and compare the model evidence of the group DCM, and identify the most likely relationship between MRS values and synaptic parameters. The ensuing neurochemistry-enriched DCM is performed in steps: after first-level DCM inversion of individual data, the resulting estimates are, effectively, used as input to group DCMs (using PEB) and re-estimated under random-effect constraints (here, using MRS data) on a subset of synaptic connections. This re-estimation uses the same calculus as Bayesian model reduction. c.f., the Savage-Dickey ratio (Friston and Penny, 2011), where the objective is to improve the free energy bound on the hierarchical model with first and second levels. We then evaluate the model evidence of PEB models where their 'covariates' are transformed MRS data for 2^N-1 combinations of N synaptic connections. We systematically evaluate which sets of synaptic parameters are informed by empirical MRS data (over all types and all combinations) and compare model evidence to select the likely connections that are evidently constrained by (a function of) MRS data. Note the MRS data furnish empirical priors, and not correlated with synaptic estimates per se.

In the following sections, we describe the multi-modal dataset (MEG and 7T-MRS) and the first-level DCM used to fit cross-spectral density data features. We then describe the second (group) level PEB model of the mapping between neurotransmitter concentration and synaptic physiology. We present the results of first-level and group-level DCMs, using MRS data as empirical priors. Finally, we discuss the potential applications and limitations of the method. A glossary and definitions of acronyms and variables used in this paper are provided in Tables 1-4.

2. Material and methods

2.1. Participants

Eleven healthy adults (age 63–77 years, five women) participated after providing written informed consent. The study had ethical approval from the Cambridge 2 Research Ethics Committee. They were free from neurological or major psychiatric disorders and took no regular medication. Each participant underwent 7T MRI and MRS (Murley et al., 2020) and task free resting-state MEG data, on separate days.

2.2. 7T MRS data

Ultra-high field magnetic resonance data were acquired using a Siemens Terra scanner at the Wolfson Brain Imaging Centre using short-echo semi-LASER sequence (repetition time/echo time = 5000/26 ms, 64 repetitions (Deelchand et al., 2015)), and VAPOR water suppression calibration (Gruetter and Tkáč, 2000). A 2 cm isotropic cubic voxel was located over the right inferior frontal gyrus (RIFG). The MRS voxel was placed using conventional anatomical landmarks by the same operator (AGM) prior to each scan. Anatomical variants (such as absent diagonal branches of the Sylvian fissure) could in principle affect voxel placement accuracy. However, there was a very close overlap of the prefrontal MRS voxels across individuals (Fig. 1 of (Murley et al., 2020)). Details of the voxel placement and MRS quality assurance metrics are provided with open access in Murley et al. (2020).

The details of the MRS processing have been reported previously in (Murley et al., 2020; Murley et al., 2022). In brief, the spectra were pre-processed to remove effects of eddy currents and frequency/phase shifts using MRspa (Dinesh Deelchand, University of Minnesota, www.cmrr.umn.edu/downloads/mrspa). The LCModel method (Version 6.2–3) was used to quantify glutamate and GABA between 0.5 and 4.2 ppm (Provencher, 1993). A MP2RAGE sequence (repetition time =4300 ms, echo time = 1.99 ms, resolution = 99 ms, bandwidth= 250 Hz/px, voxel size = 0.75 mm^3, field of view =240,240,157 mm, acceleration factor ($A>>P$) = 3, flip-angle = 5/6 and inversion times = 840/2370 ms) was

Table 1
Acronyms.

Acronyms	Description
AMPA	α-amino-3-hydroxy-5-methyl-4-isoxazolepropionic acid
BMR	Bayesian model reduction
CMM	Conductance mesoscopic model
DCM	Dynamic causal modelling
DCM for CSD	Dynamic causal modelling for cross spectral density
FT	Fourier transform
fMRI	Functional magnetic resonance imaging
$\mathcal{E}[.]$	Expectation operator
GABA	Gamma-aminobutyric acid
GLN	Glutamine
GLU	Glutamate
MEG	Magnetoencephalography
MRS	Magnetic resonance spectroscopy
NMDA	N-methyl-D-aspartate receptors
PEB	Parametric empirical Bayes
Odd/Even PSD	Power spectral density that was derived from odd or even trails in MEG data
RIFG	Right inferior frontal gyrus
SP,SS,Inh,DP	Superficial pyramidal cells, spiny stellate excitatory neurons, interneurons, deep pyramidal cells
X	Design matrix of second level model (Eq. (6)) with dimensions $n \times r$ (n subject and r covariates)
$\theta^{(1)}$	Vector of inferred parameters at first level DCM over all subjects with dimensions $np \times 1$ (n number of subjects and p number of inferred parameters in each DCM
$\theta^{(2)}$	Second level parameters with dimensions $r \times 1$ (r number of covariates)
Γ_{φ}	Scalar function of MRS data which is parametrised with a vector of parameters φ
ϕ^1	Vector of inferred parameters at first level DCM from all subjects that are influenced by MRS data.
$\Pi^{(2)}$	Precision matrix at the second level with dimensions $p \times p$ (p number of parameters at the first level)

acquired for co-registration and segmentation, using SPM12 for partial volume correction, from fractions of grey matter, white matter and CSF.

The MRS voxel size was constant across participants (2 cm isotropic). This voxel will contain varying partial tissue volumes, and derive from marginally different brain regions amongst individuals. However, we used a MRS sequence with outer voxel suppression pulses to optimise localisation and used regression analysis to correct for variation in age, sex and partial volume before modelling (see (Murley et al., 2020) for details). We used rigorous localisation standards, together with a generalised linear model to remove the effect of age, sex and correct for partial volume effects (grey matter fraction for GABA, and the grey matter and white matter fraction for Glutamate). The residual glutamate and GABA values were used for subsequent analysis (Murley et al., 2020). Note that ultra-high field MRS (7T-MRS) can better distinguish between glutamate from within the Glx "peak", and GABA, compared to high field MRS (3T-MRS).

2.3. MEG data

Resting state MEG data were collected during two recordings, each of five minute duration, on a different day to the MRS, with eyes closed using an Elekta Vector View system with 204 planar gradiometers and 102 magnetometers. MEG data were recorded continuously with 1000 Hz sampling rate. Participants' horizontal and vertical eye movements were recorded using bipolar electro-oculogram and electro-cardiogram electrodes. Five head position indicator coils were placed on an electroencephalography cap to track the head position. Three fiducial points (nasion, left and right pre-auricular) and a minimum of 100 head shape points were digitised using Polhemus digitization.

The data were pre-processed using the Elekta Neuromag toolbox (Elekta Oy), with MaxFilter v2.2.12 for detection and interpolation of bad sensors, and signal space separation to remove external noise from the data and correct for head movement correction. The data were then high-pass filtered at 1 Hz, stop-band filtered around [22 to 24] Hz and [47 to 51] Hz and divided into epochs of one second duration. We used the Field trip Toolbox (Oostenveld et al., 2011) for detection and removal of eye movement artefacts and discontinuities. Fieldtrip artefacts rejections entails Z-transforming of band-pass filtered data (between [2 15] Hz), averaging the ensuing signals over the channels, thresholding the accumulated Z-score and removing artefacts.

We applied empirical Bayesian inversion in SPM12 for source inversion and extraction of the RIFG source time series for subsequent analyses (Litvak et al., 2011). We concatenated the data of the two recordings and then divided the source data into two sets, one comprising the odd numbered epochs ('odd data') and one with the even numbered epochs ('even data') for each participant to assess the reliability of the results (Litvak et al., 2015). We separately averaged power spectral responses of the odd and even datasets. The two power spectral densities (referred to as Odd PSDs and Even PSDs) are used as the data features in the DCM of cross-spectral density.

2.4. First level analysis using dynamic causal modelling of resting states MEG data

To infer the neurophysiological parameters generating observed resting state MEG data, we used DCM for cross spectral density (CSD) in SPM12 (Friston et al., 2012; Moran et al., 2007; Moran et al., 2011). Spectral features in the resting state MEG were used to infer synpatic parameters of a biophysically-informed neural mass model, together with model evidence. DCM for CSD assumes that recorded electrophysiological oscillations are due to finite responses of neuronal dynamics, under endogenous random fluctuations (Basar et al., 2012; Haken, 1977).

We used a conductance based neural mass model as shown in Fig. 2 (known as "CMM_NMDA" model in SPM12) (Moran, 2015; Moran et al., 2013; Shaw et al., 2017). The conductance based model represents the actvity of cortical columns based on the interactions of four neuronal populations: excitatory spiny stellate cells, superfical pyramidal cells, inhibitory interneurons, and deep pryramidal cells as shown in Fig. 2.

Each population is represented by a Morris–Lecar model (Moran et al., 2013). The dynamic of each population is governed by stochastic differential equations that emulate the dynamics of pre/post-synaptic potentials, firing rates and membrane conductances. In a typical neruonal population, the dynamics of membrain potentials, V, and conductances of an ion channel, g_*, are govered by the following

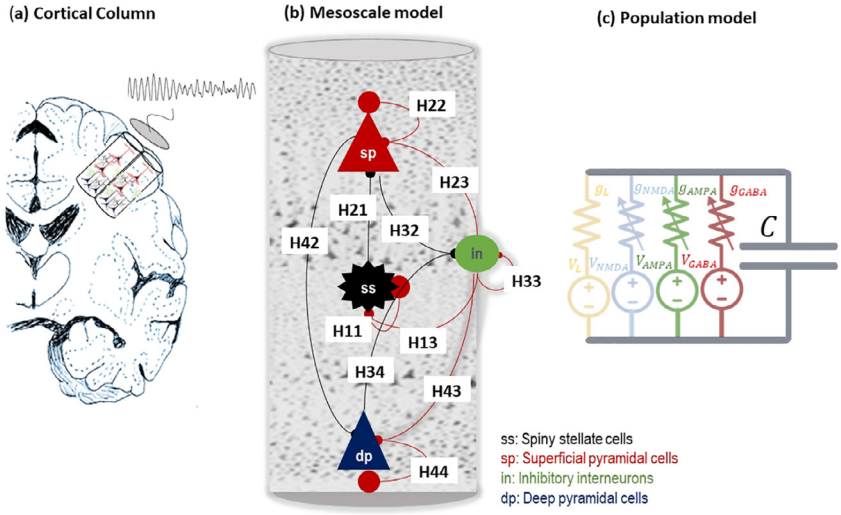

Fig. 2. The conductance based neural model. Panel (a) shows a cartoon of a cortical column which generates electrical brain activity that can be captured by neuroimaging modalities such as MEG. Panel (b) illustrates the mesoscale model which is divided into three layers where superficial (sp) and deep pyramidal (dp) cells are in the top and bottom layers, respectively, excitatory interneurons (spiny stellate cells, ss) are located in layer four, and inhibitory interneurons are distributed across all layers and are modelled using one population that interacts with all other populations. In addition, each population is equipped with a self-inhibition which assures dynamical stability around a stable fixed point. Panel (c) illustrates the population model, each neuronal population is governed by the Morris-Lecar model. This model explains the dynamics of different ion currents: NMDA, AMPA and GABA and passive ion current and membrane capacitance as explained in Eq. (1). Brain, Resistor, capacitor and voltage icons by Michael Senkow from thenounproject.com, CC BY 3.

equations:

$$\begin{aligned}\frac{dV}{dt} &= \frac{1}{C}[g_L(V_L - V) + g_{AMPA}(V_{AMPA} - V) + g_{GABA}(V_{GABA} - V) \\ &\quad + g_{NMDA}\, m(V)(V_{NMDA} - V)] + u, \\ \frac{dg_*}{dt} &= \frac{1}{\tau_*}\left(\sum_{k=sp,\ inh,\ dp,ss} H_k\, \sigma_k - g_*\right) + u, \\ &= [L_c,\ AMPA,\ GABA,\ NMDA] \end{aligned} \tag{1}$$

In Eq. (1), C is the membrane capacitance, u is random endogenous fluctuation, L_c is passive leak current where its conductance is constant, g_* is conductance associated with ion channels/receptors with time constant τ_*, $V_{AMPA,GABA,L,\ NMDA}$ are the reversal equilibrium potentials of the ion channels. The $m(V)$ in Eq. (1) represents the actvity-dependent magnesium channels which is given by $m(V) = \frac{1}{1+0.2\ exp(-\alpha_{NMDA}\, V)}$. The term σ_k in Eq. (1) is the non-negative afferent presynaptic firing from population k, which is scaled by afferent intrinsic connectvity H_k.

The scaled presynaptic firing rates are a proxy for neurotransmitter levels measured by MRS. Therefore, we hypothesise a relation between the MRS glutamate and GABA measures and excitatory and inhibitory H_k connections, which scale presynaptic actvity. In other words, the MRS glutamate and GABA can be used as empirical priors on excitatory/inhibitory connections in the generative model.

Mathematically the temporal dynamics of the conductance based model can be written in the canonical form of a dynamical system as follows (Friston et al., 2012):

$$\dot{x} = f(x, \theta) + u(\theta) \tag{2}$$

Where θ denotes a vector of all unknown parameters (i.e., H_k,τ_k), x is the state of neuronal populations in the model, $f(x, \theta)$ is a function that is the concatenated version of the right hand sides of Eq. (1)—over all populations—and u represent endogenous fluctuations, conventionally modelled by (structured) pink noise. The noise in Eq. (2) has a cross-spectrum $g_u(\omega, \theta) = FT(\mathcal{E}[u(t), u(t-\tau)])$ (Fourier transform is denoted by FT and $\mathcal{E}$ is the expectation operator).

One can approximate the dynamics of Eq. (2) with the (first order) linearised model $\dot{x} = (\nabla_{x^*} f_\theta)x + u$ (∇_{x^*} denotes the Jacobian at x^*) with the spectral response:

$$K(\omega,\ \theta) = FT\left(\exp \tau \cdot\ \nabla_x f(x, \theta)\right) \tag{3}$$

Given the spectral response of the system, the generative model of neuronal activity, $g_x(\omega)$, can be calculated as follows:

$$g_x(\omega) = K(\omega,\ \theta) \cdot g_u(\omega,\ \theta) \cdot K(\omega,\ \theta)^T +\ g_o(\omega, \theta) \tag{4}$$

In Eq. (4), $g_o(\omega, \theta)$ represents the spectrum of the observation noise, which is a sum of common and source specific noise. The spectral response in sensor space can also be generated by inclusion of a forward electromagnetic model into Eq. (4), which is denoted by L. $M(\omega)$ (L is the gain and M is the head model), as follows:

$$g_y(\omega) = L.\ M(\omega) \cdot\ g_x(\omega,\ \theta) \cdot M^T(\omega).L^T + \epsilon \tag{5}$$

In Eq. (5), $g_y(\omega)$ is the cross spectra of the MEG data and $\epsilon \sim N(0, \sigma)$ is a random effect (with unkown covariance). Because we perform the DCM analysis in source space, the forward electromagnetic model in this case just applies a scaling parameter. In the DCM, we do not predefine which neuronal population(s) contribute to MEG data. Instead, we estimated the degree to which each population (e.g. superficial, deep pyramidal or inhibitory population) contributed to the generation of the MEG data -see (Pereira et al., 2021) for details specific to conductance based models. Recently clinical and interventional applications support this approach (Adams et al., 2021; Shaw et al., 2021; Gilbert et al., 2016; Symmonds et al., 2018).

The unkown parameters in the DCM are specified as log-scale values. This means that the parameter vector in DCM is a random variable, which is given by $\theta = \theta_0 \exp(\hat{\theta})$. Here, θ_0 is a biologically informed scaling for the parameter and $\hat{\theta}$ is a random variable, with prior normal density $\hat{\theta}_0 \sim N(0,\ \sum_\theta)$ of zero mean and covariance $\sum_\theta$. This expresses the belief about the range over which parameters can vary. Note that scale parameters of this sort cannot be less than zero; for example, distances and lengths or rate and time constants or precisions and variances.

2.5. Second level analysis: group DCMs informed by empirical priors

In many translational neuroscience studies, the goal is to test hypotheses at the group level, where subject-specific information is given by summary statistics. In PEB, this subject-specific information is the posterior over key model parameters at the first level (Zeidman et al., 2019a; Zeidman et al., 2019b; Friston et al., 2015; Friston et al., 2016). At the second level the objective is to test whether synaptic connections depend on between subject variables, such as age, disease-severity, genetics, diffusion tensor imaging and MRS (Friston et al., 2016). In other words, PEB seeks to explain intersubject variability on one or more first level model parameters.

Mathematically, we denote a vector of model parameters at the first level DCM, over all participants, by a column vector $\theta^{(1)}$ (superscript '1' denotes the first level analysis) with dimension $np \times 1$ (n number of participants and p is the number of parameters for each participant). Then the generative model of the group is given by (Friston et al., 2016):

Table 2
Glossary of variables and expressions in conductance-based mesoscale model.

Variable	Description
u	Exogenous input (scalar) to membrane equation and conductance equation in each population.
V	Mean depolarisation of a neuronal population. It is a scalar variable per each population.
$\sigma(v)$	The neuronal firing rate (scalar function) – a sigmoid squashing function of depolarisation
L	Lead field vector mapping from (neuronal) states to measured (electrophysiological) responses
$g_x(\omega), g_o(\omega), g_y(\omega)$	Spectral density of (neuronal) state fluctuations, observation noise and measurement, respectively. These are vector valued functions.
$\nabla_x f$	System Jacobian or derivative of system flow with respect to (neuronal) states (matrix valued function).
$k(t) = FT[K(\omega)]$	First order kernel mapping from inputs to responses; c.f., an impulse response function of time. This is the Fourier transform of the transfer function.
$K(\omega) = FT[k(t)]$	Transfer function of frequency, modulating the power of endogenous neuronal fluctuations to produce a (cross spectral density) response. This is the Fourier transform of the kernel.

Table 3
Parameters of the neuronal model (see also Eq. (1) and Fig. 2).

	Description	Parameterisation	Prior
τ	Rate constant of ion channels	$\exp(\theta_\tau) \cdot \tau\tau = [256, 128, 16, 32]$	$p(\theta_\tau) = N(0, 1/16)$
C	Membrane capacitance	$\exp(\theta_c) \cdot CC = [128\ 128\ 256\ 32]/1000$	$p(\theta_c) = N(0, 1/16)$
H	Intrinsic connections	$\exp(\theta_H) \cdot H = \begin{bmatrix} 8\,0\,2\,0 \\ 4\,8\,8\,0 \\ 0\,0\,32\,128 \end{bmatrix}$	$p(\theta_{Ha}) = N(0, 1/32)$

$$
\begin{aligned}
y^{(i)} &= H_{\theta^{i,1}}\left(x^{(i)}\right) + \epsilon^{(i)}, \quad i = 1, .., n \\
\theta^{(1)} &= (X \otimes I)\theta^{(2)} + \epsilon^{(2)}, \quad \theta^{(1)} = \left[\theta^{i,1}, \ldots, \theta^{i,n}\right]
\end{aligned} \tag{6}
$$

The first line of Eq. (6) is the collective generative models of first level DCMs over the n subjects neuroimaging data (y denotes to generic data features in time or frequency domain, and H denotes an operator that links the activity of mesoscale model-generated by hidden subject specific hidden states $x^{(i)}$-to relevant data features). The second line is the random effects model of parameters that impose constraint on the first level parameters conventionally through empirical prior. In the second line of Eq. (6) (aka random effect model of first level synaptic connections), $X \in R^{n \times r}$ is the design matrix with $r \geq 1$ covariant (the first regressor of X is always equal to one and reflects the group mean) and a column vector $\theta^{(2)}$ (superscript '2′ denotes the second level) contains the second level parameters. The symbol $\otimes$ is the Kronecker product and I is the $p \times p$ identity matrix. The random effects have a Gaussian distribution $\epsilon^{(2)} \sim N(0, \Pi^{(2)})$ (where $\Pi^{(2)}$ is precision matrix or inverse of the covariance). The precision matrix is parameterised with a single (hyper-precision) parameter, γ, as follows (Friston et al., 2016):

$$
\Pi^{(2)} = I_S \otimes \left(Q_0 + e^{-\gamma}\, Q_1\right) \tag{7}
$$

In Eq. (7), $Q_0 \in R^{p \times p}$ is the lower bound on the precision, defined with a small positive value). The (hyper)parameter, γ, scales a precision matrix $Q_1 \in R^{p \times p}$, which is (by default) 16 times the prior precision of the group mean (Zeidman et al., 2019b): this hyperprior ensures that random effects are small in relation to prior uncertainty about the parameter in question.

The critical question is whether an alternative prior increases or decreases model evidence (Friston et al., 2016). This is an optimisation problem, where the objective function is the free energy of the PEB model. Inversion of the hierarchical model is computationally expensive if all parameters of the first level need to be inferred every time the second level parameters change (Raman et al., 2016). However, BMR can be used to re-evaluate first level posteriors under updated second level parameters (Friston et al., 2016; Litvak et al., 2015). This significantly improves the efficiency of the inversion for PEB models.

2.6. Investigating relation between MRS and synaptic connections

2.6.1. Problem setting

We test whether excitatory and inhibitory synaptic connections depend on (i.e., are functions of) glutamate and GABA measures, respectively. We used PEB to specify and compare the evidence for different functions of MRS measures, as illustrated in Fig. 3.

To identify which synaptic parameters were sensitive to neurotransmitter levels, we grouped the inferred synaptic connections into excitatory and inhibitory subsets. In detail, for the l_{ex} (l_{Inh}) excitatory (inhibitory) connections in the neural mass model, we define $2^{l_{ex}} - 1$ ($2^{l_{Inh}} - 1$) different possible combinations. The ensuing subsets of the connections (over all participants) are considered as the dependent variable of the PEB model (i.e., the right-hand side of the second line in Eq. (6)). This model encodes a hypothesis about the relationship between some (subset) connections, $\phi^{(1)} = \{\phi_i\}^k_{i=1}$ and a particular function of MRS data: $\Gamma_\varphi(MRS)$ (where Γ is a smooth and monotonic function with unknown parameters, φ). The generative model of PEB can be re-written as follows:

$$
\begin{aligned}
y^{(i)} &= H_{\theta^{i,1}}\left(x^{(i)}\right) + \epsilon^{(i)}, \quad i = 1, .., n \\
\phi^{(1)} &= \left(\left[1\ \Gamma_\varphi(MRS)\right] \otimes I\right)\phi^{(2)} + \epsilon^{(2)}, \quad \phi^{(1)} \subseteq\ \theta^{(1)} = \left[\theta^{i,1}, \ldots, \theta^{i,n}\right]
\end{aligned} \tag{8}
$$

In the second line of Eq. (8), there are two sets of unknowns that need to be inferred; namely, *(i)* the subset of connections $\phi^{(1,2)}$ (superscript 1 and 2 denotes to first and second level parameters, respectively) and *(ii)* the function or map $\Gamma_\varphi(MRS)$. These unknowns are the hyperparameters in Eq. (6). To find optimal hyperparameters, we recursively select subsets of synaptic connections and estimate the MRS function parameters, such that the model evidence in Eq. (6) is maximised. In other words, for any combination of synaptic parameters, we seek the MRS-informed PEB model with the highest evidence, using BMR. This allows us to identify the most likely solution (in terms of model evidence) from the model space tested (a set of potential monotonic relationships), to identify which set of synaptic parameters are informed by MRS data.

To assess the reproducibility of the results, given M/EEG data from a given cohort under matched conditions, we separately tested the relationship between inferred synaptic parameters and MRS by splitting the MEG data into odd and even numbered epochs (odd data and even data based validation by means of a held-out dataset). The ensuing procedure is shown in Fig. 4.

2.7. Functional form of the empirical MRS priors

The functional form of the MRS mapping is not known *a priori*. We therefore limit the search space over the MRS transformations to continuous and monotonic polynomial maps and sigmoid nonlinear functions, which cover a wide range of linear and nonlinear forms. The class of polynomials provides an approximation (Bishop, 2006) to any nonlin-

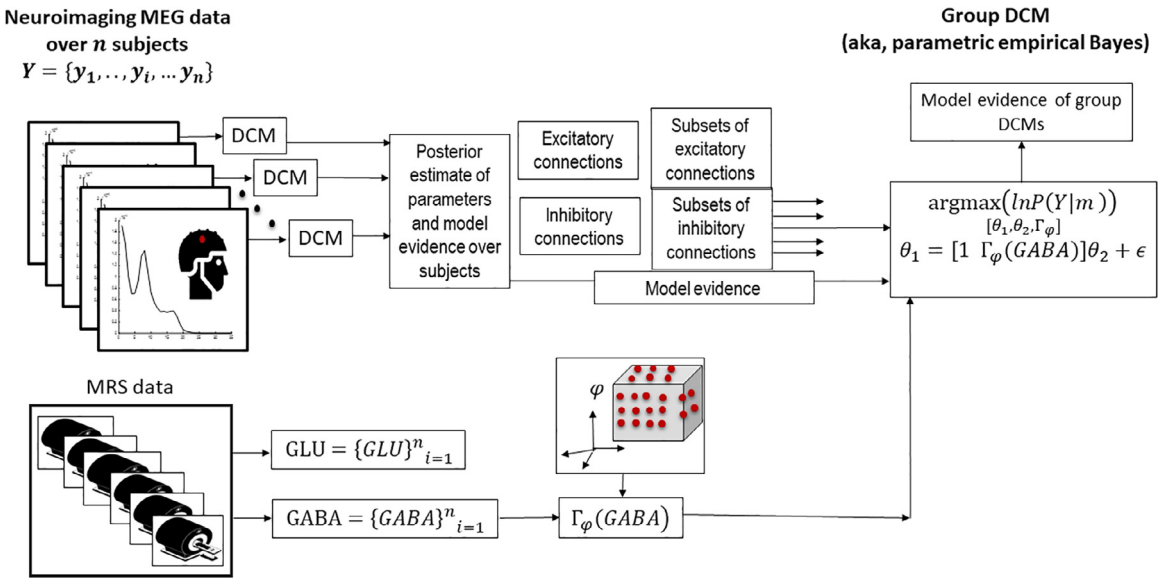

Fig. 3. MRS informed group DCM for MEG. This graphic illustrates a group DCM (aka PEB model) inversion using MRS data as empirical priors. First level DCM (left side of panel) infers synaptic physiology from each participants' data. A function of MRS glutamate (GLU) or GABA measures (bottom panel) are considered as empirical priors for certain parameters in the group DCM (right panel). Bayesian model reduction evaluates the effect of empirical priors and evaluates the model evidence for the group DCM. The objective is to find the optimal function of MRS measures—that inform synaptic parameters in the CMM-NMDA model—by maximising PEB model evidence. Image credit for the MRI scanner icon by Grant Fisher, TN from thenounproject.com, CC BY 3.

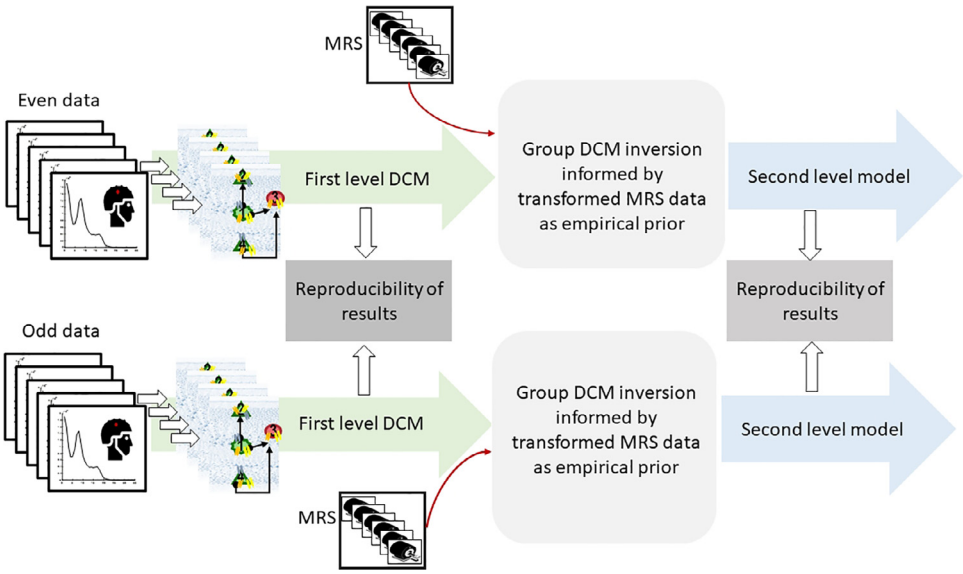

Fig. 4. Reproducibility-check procedure. The MEG data for each participant is divided into two separate datasets, 'odd data' and 'even data'. DCM for MEG is used to infer synaptic parameters for each. A post hoc correlation analysis is used to test agreement between the ensuing estimates. Parameter estimates that are consistent over the datasets are considered for further analysis. We perform the group-level inversion informed by MRS data for odd and even datasets on the selected parameters and explore which sets of connections are best informed by a function of MRS data. Finally, we compare the outcome of the PEB inversion and check the consistency of the results between the odd data and even data. MRI scanner icon by Grant Fisher, TN from thenounproject.com, CC BY 3.

ear monotonic form (Spivak, 2020):

$$\Gamma_\varphi(MRS) = \sum_{i=1}^{n} \varphi_i (MRS)^i \tag{9}$$

Here, φ_i are n unknown hyperparameters that need to be inferred by finding the values that maximise model evidence. This class of functions express different nonlinear relations including saturations (Stephan et al., 2009; Stefanovski et al., 2019), $n = 1$ implies a linear transformation of the MRS data.

Animal experiments suggest that changes in GABA and glutamate concentrations are related to neuronal responses via a sigmoid relationship (Benardete and Kriegstein, 2002; Dyke et al., 2017; Chebib et al., 2009). The general form of a sigmoid nonlinearity can be parameterised as follows:

$$\Gamma_\varphi(MRS) = \frac{1}{1 + \exp\left(-\varphi_1 \left(MRS - \varphi_2\right)\right)} \tag{10}$$

Here, the unknown hyperparameters φ_1, φ_2 are the slope and threshold parameters of the sigmoid transformation, respectively.

2.8. Hyperparameter estimation

To estimate unknown hyperparameters, we first sorted the MRS measures from small to large values, which defined an interval of the real line (called the domain of the MRS data). We then examined the variation of the parameters under the MRS transformation. In the case of the polynomial form, we checked the monotonicity of the transformation.

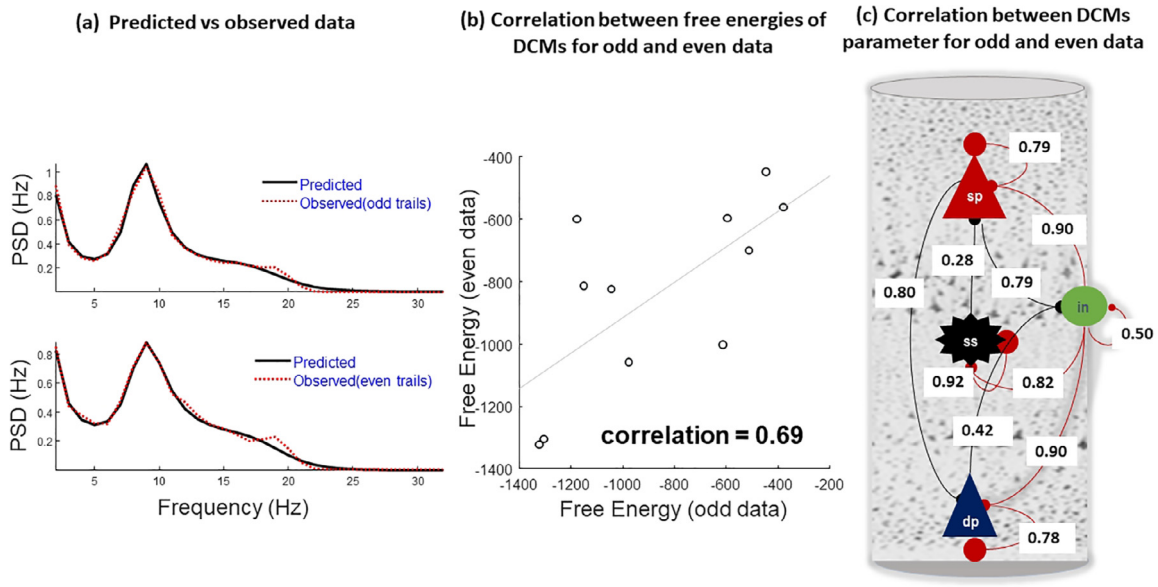

Fig. 5. First level DCM results. Panel (a) shows predicted vs observed MEG data for odd and even data from a single participant. This panel shows that DCM can explain the spectral dynamics of each dataset well. Inversion results of the rest of the subjects are provided in the supplementary material, Fig. 12. Panel (b) shows the correlation between free energies of odd and even datasets over participants (points in the plot). This correlation shows a moderately good level of agreement between the odd and even data across all participants. Panel (c) illustrates correlations between inferred synaptic connection between odd and even epochs. The inhibitory connections are shown in red and excitatory connections are shown in black.

More formally, we denoted the space of monotonic functions by $\aleph$, and defined the function γ over the ordered domain set of the MRS data to identify the range for the variation of the parameters in the polynomial function. This function has the following properties:

$$\begin{aligned} &\gamma : [\min(MRS), \max(MRS)] \to R \\ &\gamma_\varphi(.) \in \aleph \ , \quad \varphi \in \left[\min(\varphi_1) : \Delta_{\varphi_1} : \max(\varphi_1)\right] \times \ldots \times \left[\min(\varphi_n) : \Delta_{\varphi_n} : \max(\varphi_n)\right] \\ &\gamma_\varphi(MRS) = \Gamma_\varphi(MRS) \end{aligned} \tag{11}$$

Each parameter in the γ map, φ_i, varies with resolution (or step-size) Δ_{φ_i}. Note that γ_φ and Γ_φ have the same functional forms but with continuous and discretised domains. Having established the appropriate ranges (see Table 4), we used a hierarchical scheme to estimate the parameters of the map, $\Gamma_\varphi(MRS)$. For each set of synaptic connections, we calculated the model evidence—using BMR—for different values of the hyperparameters over the interval $[\min(\varphi_1) : \Delta_{\varphi_1} : \max(\varphi_1)] \times \ldots \times [\min(\varphi_n) : \Delta_{\varphi_n} : \max(\varphi_n)]$. This constitutes an exhaustive grid search. This was followed by a constrained Newtonian search, within the neighbourhood of the selected grid point, to identify the precise value of the hyperparameters that maximised model evidence. We repeated this hyperparameter optimisation over all possible subsets of the synaptic connections and selected the combinations with the greatest model evidence.

3. Results

3.1. DCM for MEG

The spectral activity from both datasets per participant (even and odd data) are used as the data features for DCM for cross spectral density to infer the parameters of the conductance based canonical microcircuit. The predicted and observed data are provided in the supplementary material Figure 12. Over all subjects, the mean variance of observed CSDs explained by the predicted CSD was 98%. The comparison of predicted and observed spectral data shows that the synaptic parameter estimates can replicate the spectral patterns of both even and odd data; with an example shown in Fig. 5 (see the supplementary material for the remaining comparisons). The correlation between the single-subject free energies associated with DCM inversions of odd/even PSD data is shown in Fig. 5.

To confirm the predictive validity of DCM, we calculated the correlation between the inferred synaptic parameters from odd and even PSDs data sets: see Fig. 5. Most parameters were estimated reliably (Fig. 5). There were exceptions, such as the excitatory connections of the deep pyramidal and inhibitory connections and superficial pyramidal cells and inhibitory cells. The low correlation between estimates of some parameters is not surprising for complex nonlinear models with conditional dependencies amongst parameter estimates (Litvak et al., 2019). It implies that different combinations of synaptic parameters may generate similar physiological data. This means hypotheses may therefore be better tested in terms of model comparison, rather than focussing on maximum, *a posteriori* parameter estimates of single parameters (Rowe et al., 2010). In the following section, we use the reliable connections—with a correlation of greater than one half—to examine the effect of neurotransmitter concentrations as measured by MRS.

Table 4
Parameterisation of MRS GABA (variable g) and glutamate (variable s) transforms.

Functional description	Parameter range
$\Gamma_\varphi(g) = \frac{1}{1+\exp(-30\exp(\varphi_1)(g-\exp(-5)\exp(\varphi_2)))}$	$\varphi_1 \times \varphi_2 = [-2 : 0.1 : 2] \times [-1 : 0.1 : 3]$
$\Gamma_\varphi(g) = \varphi_1 g + \varphi_2\, g^2$	$\varphi_1 \times \varphi_2 = [-10 : .5 : 10] \times [-10 : .5 : 10]$
$\Gamma_\varphi(s) = \frac{1}{1+\exp(-10\exp(\varphi_1)(s-\exp(-1)\exp(\varphi_2)))}$	$\varphi_1 \times \varphi_2 = [-5 : .1 : 5] \times [-4 : .1 : 0]$
$\Gamma_\varphi(s) = \varphi_1 s + \varphi_2\, s^2$	$\varphi_1 \times \varphi_2 = [-10 : .5 : 10] \times [-10 : .5 : 10]$

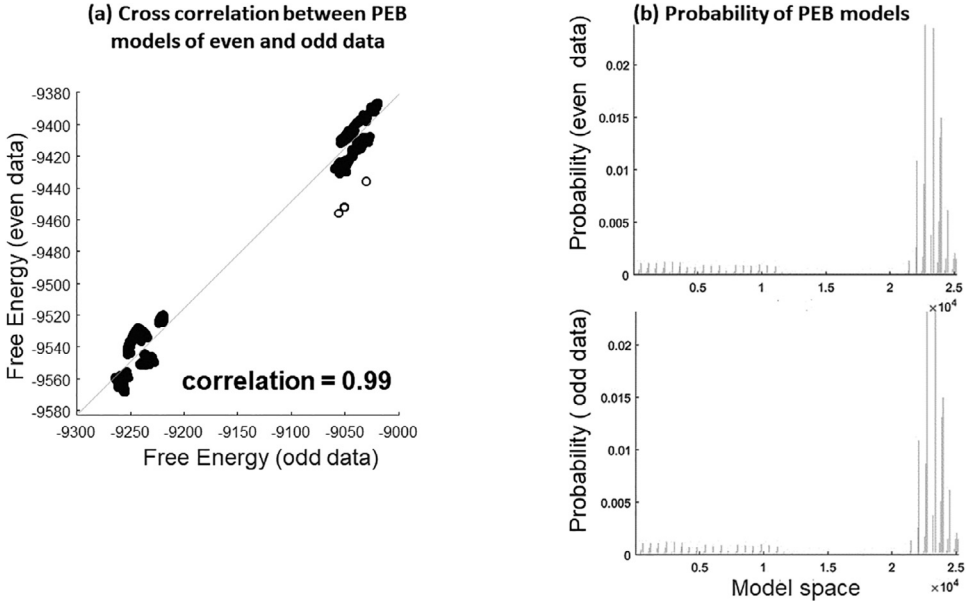

Fig. 6. Correlation analysis, comparing the free energy of the PEB model over all subsets of self-inhibitory connections and all sigmoid transformations of GABA in odd and even data. This plot shows that the PEB approach consistently estimates the marginal likelihood of models in even and odd data. (b) The probability of different PEB models over model space. Both results show the same maximum. Due to having a large model space, the probability of models and the effect sizes (free energy) are small (this is known as model dilution).

3.2. Associations between synaptic parameters and MRS measures

The most likely relationship between the synaptic parameters and neurotransmitter levels was identified through the hyperparameter optimisation.

3.3. MRS-GABA data as an empirical prior on inhibitory synaptic parameters

MRS GABA could be evaluated as an empirical prior constraint on 127 combinations of inhibitory connections (2^7–1, combinations of seven inhibitory connections in the conductance based canonical microcircuit model). As each combination might be constrained by empirical MRS GABA priors, Bayesian model reduction can be used to assess which of the 127 combinations and linear/nonlinear transformations of MRS GABA measures maximise model evidence. Alternatively, one can group certain synaptic parameters based on their common features (self-inhibition vs inter-regional connections or superficial vs deep connections), to identify the winning model 'family' for each subgroup of connections.

We grouped the inhibitory connections into four self-connections and three inter-lamina connections. By grouping the parameters in this way, we ask whether MRS GABA influences recurrent intra-laminar connectivity, or inhibition between layered populations. We assess the evidence for GABA effects, as mediated through second order polynomial and sigmoid transformations of the MRS measures. We systematically varied the hyperparameters of the sigmoid function for each subset of self-inhibitory synaptic connections and compared the resulting model evidence.

Fig. 6 shows the consistency of the resulting free energy over odd and even epoch datasets. The correlation plot between the free energies of odd and even data models shows that the ranking of model evidence is consistent, where each 'model' is a hypothesis about how MRS data supplies prior constraints on synaptic parameters. Such agreement is an important validation of hypothesis testing, based on selecting models with the greatest evidence. Using PEB to make inferences at the between-subject level inherits this validity. The high reliability suggests that both group inversions converge to the same (global) minima. For each subset of self-inhibitory connections, the sigmoid MRS GABA hyperpriors maximised the model evidence. The winning models for each subset were then examined to determine which MRS mapping is most likely for each subset of self-inhibitory connections. As shown in Fig. 7, priors using a sigmoid transformation of GABA concentration provided the most likely account of inter-subject variation in synaptic connectivity; specifically, the recurrent connections or self-inhibition of superficial and deep pyramidal cells.

We repeated the same procedure with inter-laminar (i.e., intrinsic, between population) connections. The results are shown in Figs. 8 and 9. MRS GABA provided an informative empirical prior for all inhibitory connections. The MRS transforms for odd and even datasets differ, but are similar in their functional form.

We repeated this procedure using a second order polynomial (the first order polynomial is contained within this model space) as the functional form (see supplementary material). We then compared the evidence of the winning models in each analysis; namely, the evidence for the mapping between (sigmoid MRS, self-inhibition), (sigmoid MRS, inter regions), (polynomial MRS, self-inhibition) and (polynomial MRS, inter regions), as shown in Fig. 10. The results suggest that the sigmoid transformation is the most likely functional form to explain inter-subject variability in the inhibitory recurrent (self) connections in superficial and deep layers.

3.4. MRS glutamate data as an empirical prior for excitatory synaptic parameters

We performed the proposed analysis to identify the relationship between glutamate concentration and excitatory synaptic connections. We considered different combinations of the excitatory connections over sigmoid and second order polynomial functional forms of the relationship between MRS and synaptic parameters. The correlations of models' free energy over odd and even data is shown in Fig. 11. The winning model over the complete search space confirms that MRS glutamate is linked to excitatory connections from superficial to deep layers and superficial to inhibitory interneurons (model 3).

The results of comparing a polynomial form and sigmoid transformation of MRS-glutamate measures indicate that a sigmoid transformation is overwhelmingly more likely (specifically, a sigmoid transformation of MRS glutamate measures informs the excitatory connections between deep and superficial layers, with posterior probability near unity).

4. Discussion

We present a framework for specifying and comparing hypotheses of the relationship between synaptic physiology and neurotransmitter lev-

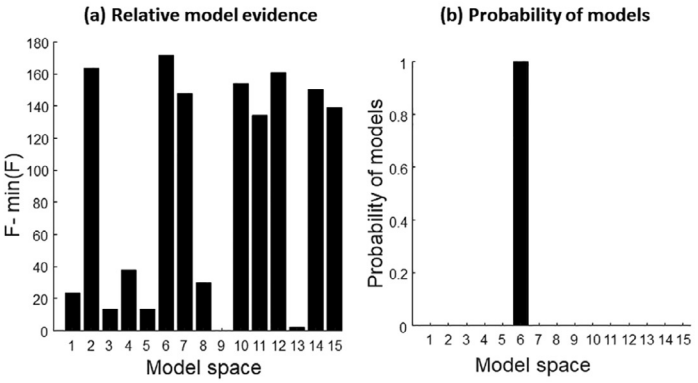

Model	synaptic connections
1	H11
2	H22
3	H33
4	H44
5	H33, H44
6	H22, H44
7	H22, H33
8	H11, H44
9	H11, H33
10	H11, H22
11	H11, H22, H33
12	H11, H22, H44
13	H11, H33, H44
14	H22, H33, H44
15	H11, H22, H33, H44

Fig. 7. (a) The relative free energy of each subset of the self-inhibitory connections. (b) the probability of each model. The most likely "winning" model is 6 in which a prior of the sigmoid transformation of MRS GABA informs connections self-inhibition of superficial and deep pyramidal cells. Please see Fig. 2 for the definitions of the connections specified within each model.

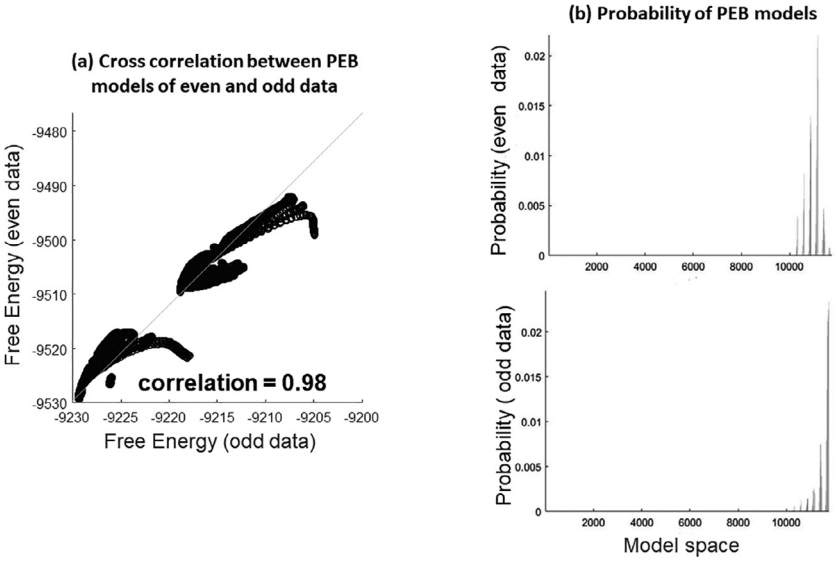

Fig. 8. (a) This panel shows a correlation analysis between the free energy from the PEB model that encodes the relationship between all possible inter-regional inhibitory synaptic connections and all possible forms of sigmoid transformation of the MRS-GABA. These results suggests that the PEB approach reliably estimates model evidence in even and odd data. (b) The probability of different PEB models over model space. The maxima in the probability plots are not consistent due to the fact that there are two different MRS transformations with the greatest evidence for the odd and even data. The maximum probability in each plot is associated with the same combination of inhibitory connections.

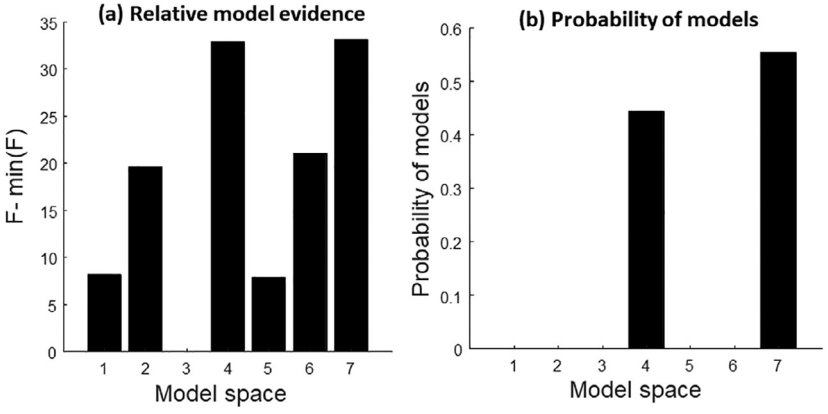

Model	synaptic connections
1	H13
2	H23
3	H43
4	H13,H23
5	H13,H43
6	H23,H43
7	H13,H23,H43

Fig. 9. (a) The relative free energy for each subset of inter-laminar inhibitory connections for an optimal transformation is shown (b) The probability of each subset of synaptic connections is illustrated. The winning model identifies that a sigmoid transformation of MRS-GABA measures is likely to inform all inter-laminar inhibitory connections. Please see Fig. 2 for the definitions of the connections specified within each model.

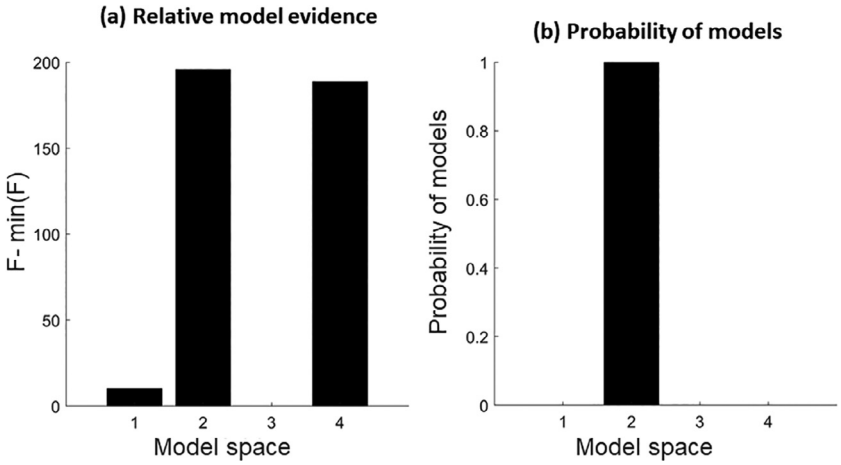

Fig. 10. Comparing the probability of sigmoid and second order models that encode the mapping from MRS GABA to self- inhibitory connections (model 2, 4) and interlaminar inhibitory connections (model 1,3). The comparison indicates the second model is most likely: a sigmoid transformation of MRS GABA informs the recurrent or self-inhibition of deep and superficial populations.

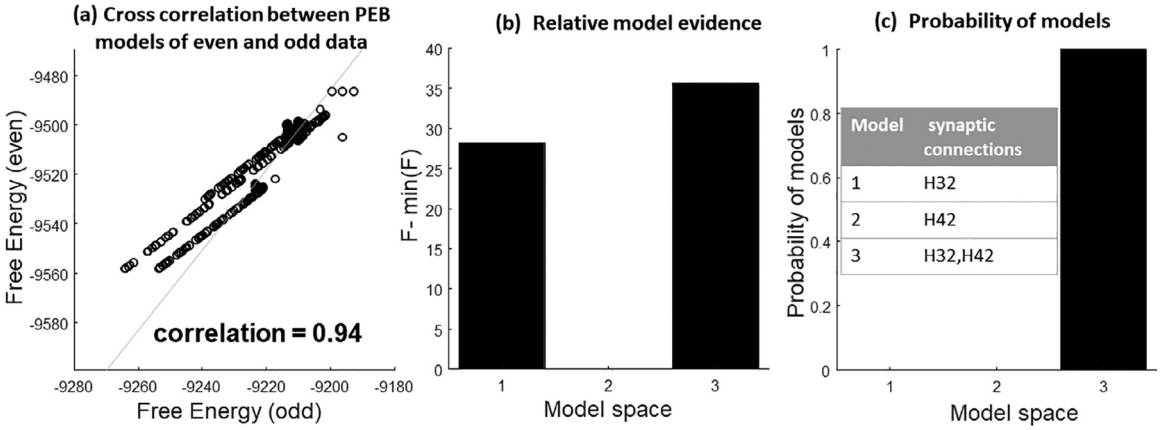

Fig. 11. (a) Correlation analysis between the free energy of the PEB model for odd and even data. This plot shows that the PEB approach consistently evaluates model evidence in even and odd data. (b) Free energy and probability of models for the odd and even data are illustrated. Model 1 includes effects on excitatory connections from superficial to deep layers, model 2 considers excitatory connections from superficial excitatory populations to inhibitory interneurons, and model 3 includes both. (c) The MRS measured glutamate that gives the maximum evidence for the odd and even data. Although, there are two MRS functions that maximise model evidence for the odd and even data, both maps suggest similar nonlinear thresholding of glutamate measures provide plausible empirical priors. Please see Fig. 2 for the definitions of the connections specified within each model.

els, based on a combination of resting-state MEG and MRS. This enables one to specify and compare the effect of biomarkers of inter-subject variation as informative priors on synaptic parameters in a time efficient and Bayes-optimal manner. The method is applicable to generative models of evoked and resting- state time series, recorded by magnetoencephalography, electroencephalography or functional magnetic resonance imaging techniques. In principle, the individual differences specified here by MRS could be replaced by other imaging modalities, or regional neuropathology assays.

We illustrate how the method can be used to test, non-invasively, hypotheses about the relationship between synaptic physiology and neurotransmitter concentrations in humans. This goes beyond the correlation between M/EEG data features and MRS estimates of neurotransmitter concentration (McColgan et al., 2020), in using formal, generative models of the neurophysiological observations. It is computationally efficient, using first level DCM once and re-evaluating the DCM parameters and model evidence analytically using Bayesian model reduction. The model evidence is thereby compared between models with and without the MRS priors, in contrast to the reinversion of the DCMs for alternative priors (Stephan et al., 2009).

We provide evidence that a non-linear transform of the MRS GABA measures offers the best explanation for inter-subject variability in inhibitory recurrent (i.e., self) connectivity of superficial and deep neuronal populations. In addition, a sigmoid transform of the MRS glutamate provides the best explanation of inter-subject variations in excitatory connections from superficial to deep layers. The identification of a sigmoid form for the MRS transform is interesting, because experimental changes of GABA and glutamate concentrations exhibit a sigmoid relationship to neuronal responses, though postsynaptic gains (Benardete and Kriegstein, 2002; Dyke et al., 2017; Chebib et al., 2009). The relationship between superficial and deep layer connectivity is especially relevant to studies of neuropsychiatric and neurological disorders with abnormalities in GABA and glutamate, e.g., schizophrenia, movement disorders and dementia (Adams et al., 2021; Murley et al., 2020; Murley et al., 2022). Using MRS data as an empirical prior on the synaptic connections may provide valuable information about the impact of neuropathology on synaptic function and the response to treatment.

There are several limitations to this study. We focus on the relationship between neurochemical concentrations and synaptic physiology in one cortical region. The choice of the right inferior frontal gyrus was motivated by our interest in frontal lobe function and its impairment in frontotemporal lobar degeneration (Eliasova et al., 2014; Hughes et al., 2015; Murley et al., 2020; Murley et al., 2022) and other neuropsychiatric disorders. However, the method can be applied to multiple regions. For instance, one could combine neurophysiology and spectroscopy from principal nodes in the default mode or salience networks; and test whether MRS data at different regions are associated with extrinsic (between-source) and intrinsic (within-source) connections. Such

an approach could test whether local neurotransmitter concentrations in one source influence the activity and connectivity of other sources. The spatial resolution of MRS data is limited. The average neurotransmitter concentrations are captured over multiple cortical columns. Here, the GABA estimate is used as a marker of between-subject differences in neurotransmitters for the lateral frontal cortex. We assume that the voxel-wise estimate approximates the neurochemical concentrations in the neurophysiological source used to extract time series for DCM inversion, noting that the source lies within the MRS voxel (Murley et al., 2020).

Our study size was modest, although similar to (Stephan et al., 2009), where a related method for DCM is described. A larger sample size could widen the intersubject distribution, and facilitate the inversion of the hierarchical models (Kerkhoff and Nussbeck, 2019). However, the Bayes factors indicate that our study had sufficient precision (sufficient 'power' by analogy to frequentist testing) to support the inferences made. Although we draw inferences about the role of GABA and glutamate on neurophysiological function, and synaptic connectivity specifically, we do not, in this study, perturb such functions through psychopharmacological challenges. The combination of the current analysis with GABAergic or glutamatergic interventions could be used to identify baseline dependent effects of drug interventions, as in (Adams et al., 2021) within a simpler and integrated Bayesian modelling procedure.

In this paper, we demonstrate a proof of principle for leveraging neurotransmitter levels in neuronal modelling through a hierarchical Bayesian approach. The use of PEB well-suited for neurochemistry-enriched DCM, as it addresses whether models with weakly-informative priors or models with empirical priors on parameters lead to higher model evidence (with an implicit penalty for model complexity). We illustrate how this method could be used to test (non-invasively) alternative hypotheses about the association (in terms of empirical prior) between synaptic physiology and neurotransmitter concentrations in humans. GABA and glutamate priors increase model evidence when applied to inhibitory and excitatory synapses connectivity respectively. The data splitting was useful for establishing the reliability of model comparison and parameter estimation, when applied to separate data acquired from the same subjects under matched conditions (odd-versus even trials- aka validation by means of a held-out dataset). Other forms of validation could be considered, including predictive validation by drug intervention (e.g., by a GABA-ergic drug) or post-mortem biochemistry. Note that we focussed here on glutamate and GABA priors for synaptic connections, because of the clear predictions related to excitatory and inhibitory synaptic function respectively, and that we do not recommend arbitrary or non-plausible priors (Friston et al., 2013).

We performed a greedy search over the MRS map's parameter space using a fine resolution, which may have contributed to the smooth changes in Free energies in Figs. 6 to 10. In other words, it may be possible to reach the optimal solution even with coarser discretisation of the search space. A further potential limitation to our modelling is the lack of knowledge about MRS data variability in the control cohort. In addition, non-simultaneous multimodal data acquisition raises the question of non-stationarity, or within-subject variance, as a potential confound. A crucial issue is whether the variance within-subject between-assessments is large or small compared to between-subject variance. Several studies suggest that under no-task or easy-task conditions, MRS has excellent test-retest reliability (Wiehler et al., 2022; Prinsen et al., 2017; Terpstra et al., 2016; Gawne et al., 2020). Variation in GABA or glutamate levels between MRS and the MEG recording would (for classical statistics) increase type II error (i.e., reduce power) or (for Bayesian statistics) reduce precision and the ability to draw definitive inferences from model comparison.

In conclusion, we propose that dynamic causal models of neurophysiology can be explicitly informed by priors based on measures of individual differences in neurochemistry, molecular pathology or cell/synapse specific loss. The enrichment of DCMs by such markers of inter-subject variability has many potential applications, exploiting the computational efficiencies of parametric empirical Bayesian methods and Bayesian Model Reduction with hierarchical inversion of individual and group-level models of functional imaging data.

Author contribution

Amirhossein Jafarian: Conceptualization, Methodology, Software, Validation, Formal analysis, Writing Original Draft, Data Curation, Visualization.

Laura Hughes: Max-filtering software, Review & Editing.

Natalie E Adams: Discussion, Review & Editing.

Michelle Naessens: Data collection, Review & Editing.

Matthew A Rouse: Data collection, Review & Editing.

Juliette Lanskey: Discussion, Review & Editing.

Alexander G Murley: MRS Data Collection, Review & Editing.

Karl J Friston: Conceptualization, Methodology, Review & Editing, Supervision.

James B Rowe: Conceptualization, Methodology, Review & Editing, Supervision, Funding acquisition.

Declaration of Competing Interest

The author declares no competing interests.

Data availability

The code associated with this paper is available at "https://github.com/NIMG-22-2183/MRS-DCM". Raw data can be requested from the senior author, noting that a data transfer agreement is likely to be required under the terms of consent and data protection legislation.

Acknowledgements

This work has been funded by the Wellcome Trust (220258), the Medical Research Council (SUAG/092 G116768) and Cambridge Centre for Parkinson-plus; the Holt fellowship; and the NIHR Cambridge Biomedical Research Centre (BRC-1215-20014). This research was also supported by the NIHR Cambridge Biomedical Research Centre (NIHR203312). KJF is supported by funding for the Wellcome Centre for Human Neuroimaging (Ref: 205103/Z/16/Z) and a Canada-UK Artificial Intelligence Initiative (Ref: ES/T01279X/1). The views expressed are those of the author(s) and not necessarily those of the NIHR or the Department of Health and Social Care. For the purpose of open access, the authors have applied a CC BY public copyright licence to any Author Accepted Manuscript version arising from this submission.

Supplementary materials

Supplementary material associated with this article can be found, in the online version, at doi:10.1016/j.neuroimage.2023.120193.

References

Adams, N.E., Hughes, L.E., Rouse, M.A., Phillips, H.N., Shaw, A.D., Murley, A.G., Cope, T.E., Bevan-Jones, W.R., Passamonti, L., Street, D., Holland, N., Nesbitt, D., Friston, K., Rowe, J.B., 2021. GABAergic cortical network physiology in frontotemporal lobar degeneration. Brain 144, 2135–2145.

Basar, E., Flohr, H., Haken, H., Mandell, A., 2012. Synergetics of the Brain: Proceedings of the International Symposium on Synergetics at Schloß Elmau. Springer Science & Business Media, Bavaria *May 2–71983*.

Benardete, E.A., Kriegstein, A.R., 2002. Increased excitability and decreased sensitivity to GABA in an animal model of dysplastic cortex. Epilepsia 43, 970–982.

Bishop, C.M., 2006. Pattern Recognition and Machine Learning. springer.

Blüml, S., Panigrahy, A, 2012. MR Spectroscopy of Pediatric Brain Disorders. Springer Science & Business Media.

Boumezbeur, F., Mason, G.F., De Graaf, R.A., Behar, K.L., Cline, G.W., Shulman, G.I., Rothman, D.L., Petersen, K.F., 2010. Altered brain mitochondrial metabolism in healthy aging as assessed by in vivo magnetic resonance spectroscopy. J. Cereb. Blood Flow Metab. 30, 211–221.

Chebib, M., Gavande, N., Wong, K.Y., Park, A., Premoli, I., Mewett, K.N., Allan, R.D., Duke, R.K., Johnston, G.A., Hanrahan, J.R., 2009. Guanidino acids act as ρ1 GABA C receptor antagonists. Neurochem. Res. 34, 1704–1711.

Chowdhury, G.M., Behar, K.L., Cho, W., Thomas, M.A., Rothman, D.L., Sanacora, G., 2012. 1H-[13C]-nuclear magnetic resonance spectroscopy measures of ketamine's effect on amino acid neurotransmitter metabolism. Biol. Psychiatry 71, 1022–1025.

Cohen, S.M., Tsien, R.W., Goff, D.C., Halassa, M.M., 2015. The impact of NMDA receptor hypofunction on GABAergic neurons in the pathophysiology of schizophrenia. Schizophr. Res. 167, 98–107.

Deco, G., Jirsa, V.K., Robinson, P.A., Breakspear, M., Friston, K., 2008. The dynamic brain: from spiking neurons to neural masses and cortical fields. PLoS Comput. Biol. 4, e1000092.

Deelchand, D.K., Adanyeguh, I.M., Emir, U.E., Nguyen, T.M., Valabregue, R., Henry, P.G., Mochel, F., Öz, G., 2015. Two-site reproducibility of cerebellar and brainstem neurochemical profiles with short-echo, single-voxel MRS at 3T. Magn. Reson. Med. 73, 1718–1725.

Duarte, J.M., Xin, L., 2019. Magnetic resonance spectroscopy in schizophrenia: evidence for glutamatergic dysfunction and impaired energy metabolism. Neurochem. Res. 44, 102–116.

Dyke, K., Pépés, S.E., Chen, C., Kim, S., Sigurdsson, H.P., Draper, A., Husain, M., Nachev, P., Gowland, P.A., Morris, P.G, 2017. Comparing GABA-dependent physiological measures of inhibition with proton magnetic resonance spectroscopy measurement of GABA using ultra-high-field MRI. Neuroimage 152, 360–370.

Eliasova, I., Anderkova, L., Marecek, R., Rektorova, I., 2014. Non-invasive brain stimulation of the right inferior frontal gyrus may improve attention in early Alzheimer's disease: a pilot study. J. Neurol. Sci. 346, 318–322.

Friston, K., Mattout, J., Trujillo-Barreto, N., Ashburner, J., Penny, W., 2007. Variational free energy and the Laplace approximation. Neuroimage 34, 220–234.

Friston, K., Parr, T. & Zeidman, P. 2018. Bayesian model reduction. *arXiv preprint arXiv:1805.07092*.

Friston, K., Penny, W., 2011. Post hoc Bayesian model selection. Neuroimage 56, 2089–2099.

Friston, K., Zeidman, P., Litvak, V., 2015. Empirical Bayes for DCM: a group inversion scheme. Front. Syst. Neurosci. 9, 164.

Friston, K.J., Bastos, A., Litvak, V., Stephan, K.E., Fries, P., Moran, R.J., 2012. DCM for complex-valued data: cross-spectra, coherence and phase-delays. Neuroimage 59, 439–455.

Friston, K., Daunizeau, Stephan, K.E., 2013. Model selection and gobbledygook: Response to Lohmann et al. In: Neuroimage, 75. Elsevier, pp. 275–278 doi:10.1016/j.neuroimage.2011.11.064.

Friston, K.J., Flandin, G., Razi, A., 2022. Dynamic causal modelling of COVID-19 and its mitigations. Sci. Rep. 12, 12419.

Friston, K.J., Harrison, L., Penny, W., 2003. Dynamic causal modelling. Neuroimage 19, 1273–1302.

Friston, K.J., Litvak, V., Oswal, A., Razi, A., Stephan, K.E., Van Wijk, B.C., Ziegler, G., Zeidman, P., 2016. Bayesian model reduction and empirical Bayes for group (DCM) studies. Neuroimage 128, 413–431.

Friston, K.J., Parr, T., Zeidman, P., Razi, A., Flandin, G., Daunizeau, J., Hulme, O.J., Billig, A.J., Litvak, V., Moran, R.J., 2020. Dynamic causal modelling of COVID-19. Wellcome Open Res. 5.

Friston, K.J., Preller, K.H., Mathys, C., Cagnan, H., Heinzle, J., Razi, A., Zeidman, P., 2019. Dynamic causal modelling revisited. Neuroimage 199, 730–744.

Friston, K.J., Trujillo-Barreto, N., Daunizeau, J., 2008. DEM: a variational treatment of dynamic systems. Neuroimage 41, 849–885.

Gawne, T.J., Overbeek, G.J., Killen, J.F., Reid, M.A., Kraguljac, N.V., Denney, T.S., Ellis, C.A., Lahti, A.C., 2020. A multimodal magnetoencephalography 7 T fMRI and 7 T proton MR spectroscopy study in first episode psychosis. NPJ Schizophr. 6, 1–9.

Gawne, T.J., Overbeek, G.J., Killen, J.F., Reid, M.A., Kraguljac, N.V., Denney, T.S., Ellis, C.A., Lahti, A.C., 2020. A multimodal magnetoencephalography 7 T fMRI and 7 T proton MR spectroscopy study in first episode psychosis. npj Schizophrenia, 6. Nature Publishing Group UK, London doi:10.1038/s41537-020-00113-4.

Gilbert, J.R., Symmonds, M., Hanna, M.G., Dolan, R.J., Friston, K.J., Moran, R.J., 2016. Profiling neuronal ion channelopathies with non-invasive brain imaging and dynamic causal models: case studies of single gene mutations. Neuroimage 124, 43–53.

Greenhouse, I., King, M., Noah, S., Maddock, R.J., Ivry, R.B., 2017. Individual differences in resting corticospinal excitability are correlated with reaction time and GABA content in motor cortex. J. Neurosci. 37, 2686–2696.

Gruetter, R., Seaquist, E.R., Ugurbil, K., 2001. A mathematical model of compartmentalized neurotransmitter metabolism in the human brain. Am. J. Physiol.-Endocrinol. Metabol. 281, E100–E112.

Gruetter, R., Tkáč, I, 2000. Field mapping without reference scan using asymmetric echo–planar techniques. Magnet. Reson. Med.: Off. J. Int. Soc. Magnet. Reson. Med. 43, 319–323.

Haken, H., 1977. Synergetics. Phys. Bull. 28, 412.

Hodgkin, A.L., Huxley, A.F., 1952. A quantitative description of membrane current and its application to conduction and excitation in nerve. J. Physiol. (Lond.) 117, 500.

Hughes, L.E., Rittman, T., Regenthal, R., Robbins, T.W., Rowe, J.B., 2015. Improving response inhibition systems in frontotemporal dementia with citalopram. Brain 138, 1961–1975.

Jelen, L.A., King, S., Mullins, P.G., Stone, J.M., 2018. Beyond static measures: a review of functional magnetic resonance spectroscopy and its potential to investigate dynamic glutamatergic abnormalities in schizophrenia. J. Psychopharmacol. 32, 497–508.

Jirsa, V.K., Stacey, W.C., Quilichini, P.P., Ivanov, A.I., Bernard, C., 2014. On the nature of seizure dynamics. Brain 137, 2210–2230.

Kass, R.E., Raftery, A.E., 1995. Bayes factors. J. Am. Stat. Assoc. 90, 773–795.

Kerkhoff, D., Nussbeck, F.W., 2019. The influence of sample size on parameter estimates in three-level random-effects models. In: Frontiers in psychology, 10. Frontiers Media SA, p. 1067 doi:10.3389/fpsyg.2019.01067.

Kober, H., Nimsky, C., Möller, M., Hastreiter, P., Fahlbusch, R., Ganslandt, O, 2001. Correlation of sensorimotor activation with functional magnetic resonance imaging and magnetoencephalography in presurgical functional imaging: a spatial analysis. Neuroimage 14, 1214–1228.

Lally, N., Mullins, P.G., Roberts, M.V., Price, D., Gruber, T., Haenschel, C., 2014. Glutamatergic correlates of gamma-band oscillatory activity during cognition: a concurrent ER-MRS and EEG study. Neuroimage 85, 823–833.

Limongi, R., Jeon, P., Theberge, J., Palaniyappan, L., 2021. Counteracting effect of glutathione on the glutamate-driven excitation/inhibition imbalance in first-episode schizophrenia: a 7T Mrs and dynamic causal modeling study. Biol. Psychiatry 89, S282.

Litvak, V., Garrido, M., Zeidman, P., Friston, K., 2015. Empirical Bayes for group (DCM) studies: a reproducibility study. Front. Hum. Neurosci. 9, 670.

Litvak, V., Jafarian, A., Zeidman, P., Tibon, R., Henson, R.N., Friston, K., 2019. There's no such thing as a 'true'model: the challenge of assessing face validity. In: 2019 IEEE International Conference on Systems, Man and Cybernetics (SMC). IEEE, pp. 4403–4408.

Litvak, V., Mattout, J., Kiebel, S., Phillips, C., Henson, R., Kilner, J., Barnes, G., Oostenveld, R., Daunizeau, J., Flandin, G., 2011. EEG and MEG data analysis in SPM8. In: Computational Intelligence and Neuroscience, p. 2011.

Marreiros, A., Pinotsis, D., Brown, P., Friston, K., 2015. DCM, conductance based models and clinical applications. In: Validating Neuro-Computational Models of Neurological and Psychiatric Disorders, pp. 43–70.

Marreiros, A.C., Kiebel, S.J., Daunizeau, J., Harrison, L.M., Friston, K.J., 2009. Population dynamics under the Laplace assumption. Neuroimage 44, 701–714.

Marreiros, A.C., Kiebel, S.J., Friston, K.J., 2010. A dynamic causal model study of neuronal population dynamics. Neuroimage 51, 91–101.

Mccolgan, P., Joubert, J., Tabrizi, S.J., Rees, G., 2020. The human motor cortex microcircuit: insights for neurodegenerative disease. Nat. Rev. Neurosci. 21, 401–415.

Moran, R., 2015. Deep brain stimulation for neurodegenerative disease: a computational blueprint using dynamic causal modeling. Prog. Brain Res..

Moran, R.J., Kiebel, S.J., Stephan, K.E., Reilly, R., Daunizeau, J., Friston, K.J., 2007. A neural mass model of spectral responses in electrophysiology. Neuroimage 37, 706–720.

Moran, R.J., Pinotsis, D.A., Friston, K.J., 2013. Neural masses and fields in dynamic causal modeling. Front. Comput. Neurosci. 7, 57.

Moran, R.J., Stephan, K.E., Dolan, R.J., Friston, K.J., 2011. Consistent spectral predictors for dynamic causal models of steady-state responses. Neuroimage 55, 1694–1708.

Murley, A.G., Rouse, M.A., Jones, P.S., Ye, R., Hezemans, F.H., O'Callaghan, C., Frangou, P., Kourtzi, Z., Rua, C., Carpenter, T.A, 2020. GABA and glutamate deficits from frontotemporal lobar degeneration are associated with disinhibition. Brain 143, 3449–3462.

Murley, A.G., Tsvetanov, K.A., Rouse, M.A., Jones, P.S., Svaerke, K., Carpenter, T.A., Rowe, J.B., 2022. Proton magnetic resonance spectroscopy in frontotemporal lobar degeneration-related syndromes. Neurobiol. Aging 111, 64–70.

Myers, J.F., Evans, C.J., Kalk, N.J., Edden, R.A., Lingford-Hughes, A.R., 2014. Measurement of GABA using J-difference edited 1H-MRS following modulation of synaptic GABA concentration with tiagabine. Synapse 68, 355–362.

Nelson, M., Rinzel, J., 1998. The Hodgkin—Huxley model. *The book of Genesis*. Springer.

Oostenveld, R., Fries, P., Maris, E., Schoffelen, J.-.M., 2011. FieldTrip: open source software for advanced analysis of MEG, EEG, and invasive electrophysiological data. In: Computational Intelligence and Neuroscience, p. 2011.

Passamonti, L., Crockett, M.J., Apergis-Schoute, A.M., Clark, L., Rowe, J.B., Calder, A.J., Robbins, T.W., 2012. Effects of acute tryptophan depletion on prefrontal-amygdala connectivity while viewing facial signals of aggression. Biol. Psychiatry 71, 36–43.

Pellerin, L., Bouzier-Sore, A.K., Aubert, A., Serres, S., Merle, M., Costalat, R., Magistretti, P.J., 2007. Activity-dependent regulation of energy metabolism by astrocytes: an update. Glia 55, 1251–1262.

Pereira, I., Frässle, S., Heinzle, J., Schöbi, D., Do, C.T., Gruber, M., Stephan, K.E, 2021. Conductance-based dynamic causal modeling: a mathematical review of its application to cross-power spectral densities. Neuroimage 245, 118662.

Prinsen, H., de, G., Robin, A., Mason, G.F., Pelletier, D., Juchem, C., 2017. Reproducibility measurement of glutathione, GABA, and glutamate: Towards in vivo neurochemical profiling of multiple sclerosis with MR spectroscopy at 7T. In: Journal of Magnetic Resonance Imaging, 45. Wiley Online Library, pp. 187–198 doi:10.1002/jmri.25356.

Provencher, S.W., 1993. Estimation of metabolite concentrations from localized in vivo proton NMR spectra. In: Magnetic resonance in medicine, 30. Wiley Online Library, pp. 672–679 doi:10.1002/mrm.1910300604.

Rae, C.L., Nombela, C., Rodríguez, P.V., Ye, Z., Hughes, L.E., Jones, P.S., Ham, T., Rittman, T., Coyle-Gilchrist, I., Regenthal, R, 2016. Atomoxetine restores the response inhibition network in Parkinson's disease. Brain 139, 2235–2248.

Raman, S., Deserno, L., Schlagenhauf, F., Stephan, K.E., 2016. A hierarchical model for integrating unsupervised generative embedding and empirical Bayes. J. Neurosci. Method. 269, 6–20.

Ramezanian-Panahi, M., Abrevaya, G., Gagnon-Audet, J.-.C., Voleti, V., Rish, I., Dumas, G., 2022. Generative models of brain dynamics. Front. Artifi. Intell. 147.

Rideaux, R., 2020. Temporal dynamics of GABA and Glx in the visual cortex. eNeuro 7.

Rideaux, R., 2021. No balance between glutamate+ glutamine and GABA+ in visual or motor cortices of the human brain: a magnetic resonance spectroscopy study. Neuroimage 237, 118191.

Robinson, P.A., Rennie, C.J., Rowe, D.L., O'Connor, S.C., Wright, J.J., Gordon, E., Whitehouse, R.W., 2003. Neurophysical modeling of brain dynamics. Neuropsychopharmacology 28, S74–S79.

Rowe, J.B., Hughes, L.E., Barker, R.A., Owen, A.M., 2010. Dynamic causal modelling of effective connectivity from fMRI: are results reproducible and sensitive to Parkinson's disease and its treatment? Neuroimage 52, 1015–1026.
Schmitz, T.W., Correia, M.M., Ferreira, C.S., Prescot, A.P., Anderson, M.C., 2017. Hippocampal GABA enables inhibitory control over unwanted thoughts. Nat. Commun. 8, 1–12.
Shaw, A., Moran, R.J., Muthukumaraswamy, S.D., Brealy, J., Linden, D., Friston, K.J., Singh, K.D., 2017. Neurophysiologically-informed markers of individual variability and pharmacological manipulation of human cortical gamma. Neuroimage 161, 19–31.
Shaw, A.D., Hughes, L.E., Moran, R., Coyle-Gilchrist, I., Rittman, T., Rowe, J.B., 2021. In vivo assay of cortical microcircuitry in frontotemporal dementia: a platform for experimental medicine studies. Cereb. Cortex 31, 1837–1847.
Shine, J.M., Müller, E.J., Munn, B., Cabral, J., Moran, R.J., Breakspear, M, 2021. Computational models link cellular mechanisms of neuromodulation to large-scale neural dynamics. Nat. Neurosci. 24, 765–776.
Sokolov, A.A., Zeidman, P., Erb, M., Ryvlin, P., Pavlova, M.A., Friston, K.J., 2019. Linking structural and effective brain connectivity: structurally informed Parametric Empirical Bayes (si-PEB). Brain Struct. Funct. 224, 205–217.
Spivak, M., 2020. Calculus: Càlcul Infinitesimal. Reverté.
Stagg, C., Bestmann, S., Constantinescu, A., Moreno Moreno, L., Allman, C., Mekle, R., Woolrich, M., Near, J., Johansen-Berg, H., Rothwell, J, 2011. Relationship between physiological measures of excitability and levels of glutamate and GABA in the human motor cortex. J. Physiol. (Lond.) 589, 5845–5855.
Stagg, C., Rothman, D., 2013. Magnetic Resonance spectroscopy: Tools for Neuroscience Research and Emerging Clinical Applications. Academic Press.
Steel, A., Mikkelsen, M., Edden, R.A., Robertson, C.E., 2020. Regional balance between glutamate+ glutamine and GABA+ in the resting human brain. Neuroimage 220, 117112.
Stefanovski, L., Triebkorn, P., Spiegler, A., Diaz-Cortes, M.-A., Solodkin, A., Jirsa, V., Mcintosh, A.R., Ritter, P., Initiative, A.S.D.N., 2019. Linking molecular pathways and large-scale computational modeling to assess candidate disease mechanisms and pharmacodynamics in Alzheimer's disease. Front. Comput. Neurosci. 13, 54.
Stephan, K.E., Tittgemeyer, M., Knösche, T.R., Moran, R.J., Friston, K.J, 2009. Tractography-based priors for dynamic causal models. Neuroimage 47, 1628–1638.
Steyn-Ross, A., Steyn-Ross, M., 2010. Modeling Phase Transitions in the Brain. Springer.
Symmonds, M., Moran, C.H., Leite, M.I., Buckley, C., Irani, S.R., Stephan, K.E., Friston, K.J., Moran, R.J., 2018. Ion channels in EEG: isolating channel dysfunction in NMDA receptor antibody encephalitis. Brain 141, 1691–1702.
Terpstra, M., Cheong, I., Lyu, T., Deelchand, D.K., Emir, U.E., Bedna, K.P., Eberly, L.E., 2016. Test-retest reproducibility of neurochemical profiles with short-echo, single-voxel MR spectroscopy at 3T and 7T. In: Magnetic resonance in medicine, 76. Wiley Online Library, pp. 1083–1091 doi:10.1002/mrm.26022.
Terry, J.R., Woldman, W., Peterson, A.D., Cook, B.J., 2022. Neural Field Models: a mathematical overview and unifying framework. In: Mathematical Neuroscience and Applications, p. 2.
Van Der Graaf, M., 2010. In vivo magnetic resonance spectroscopy: basic methodology and clinical applications. Eur. Biophys. J. 39, 527–540.
Wang, H., Tan, L., Wang, H.-F., Liu, Y., Yin, R.-H., Wang, W.-Y., Chang, X.-L., Jiang, T., Yu, J.-T., 2015. Magnetic resonance spectroscopy in Alzheimer's disease: systematic review and meta-analysis. J. Alzheimers Dis. 46, 1049–1070.
Wiehler, A., Branzoli, F., Adanyeguh, I., Mochel, F., Pessiglione, M., 2022. A neuro-metabolic account of why daylong cognitive work alters the control of economic decisions. In: Current Biology, 32. Elsevier, pp. 3564–3575 doi:10.1016/j.cub.2022.07.010.
Zeidman, P., Friston, K. & Parr, T. 2022. A primer on Variational Laplace.
Zeidman, P., Jafarian, A., Corbin, N., Seghier, M.L., Razi, A., Price, C.J., Friston, K.J., 2019a. A guide to group effective connectivity analysis, part 1: first level analysis with DCM for fMRI. Neuroimage 200, 174–190.
Zeidman, P., Jafarian, A., Seghier, M.L., Litvak, V., Cagnan, H., Price, C.J., Friston, K.J., 2019b. A guide to group effective connectivity analysis, part 2: second level analysis with PEB. Neuroimage 200, 12–25.